Polymerization of Wormlike Micelles Induced by Hydrotropic Salt

Shiyong Liu,[†] Yamaira I. González,[‡] Dganit Danino,[§] and Eric W. Kaler*,[‡]

Department of Polymer Science and Engineering, University of Science and Technology of China, Hefei, 230026, Anhui Province, P.R. China; Department of Chemical Engineering, University of Delaware, Newark, Delaware 19716; and Department of Biotechnology and Food Engineering, Technion−Israel Institute of Technology, Haifa, Israel 32000

Received November 15, 2004; Revised Manuscript Received January 5, 2005

ABSTRACT: Addition of the hydrotropic salt sodium tosylate (TSNa) to solutions of a polymerizable cationic surfactant, methacryloyloxyundecyltrimethylammonium bromide (MUTB), leads to a transition from spherical to wormlike micelles about 40 nm in length. The wormlike micelles were successfully polymerized to yield stable, single-phase solutions of polymerized micelles. The polymerized wormlike micelles were several hundred nanometers long, although their cross-sectional radius remained unchanged (∼2 nm). The spherical to wormlike micelle transition, and the wormlike micelles polymerized at different molar ratios of TSNa to MUTB, were characterized using quasi-elastic and static light scattering, small-angle neutron scattering, NMR, and cryogenic transmission electron microscopy.

Introduction

Single-tailed surfactants generally form globular micelles in aqueous solution above their critical micelle concentration. These micelles can transform into wormlike micelles with addition of inorganic (e.g., Cl^- and Br^-)[1−4] or organic counterions (e.g., salicylate,[5,6] tosylate,[7] chlorobenzoate,[8] or hydroxynaphthalene carboxylate[9]). Likewise, micelle elongation can result from increasing the surfactant concentration[10] or addition of oppositely charged surfactants[11,12] or uncharged compounds such as aromatic hydrocarbons.[13] Of special interest are the salts of organic counterions, called hydrotropes. Hydrotropes are amphiphilic molecules that become weakly surface active at high concentrations. Unlike surfactants, hydrotropes have a short tail that hinders their self-assembly into micelles.[14] On the other hand, hydrotropes bind more strongly to the surfactant headgroups in the micelles than inorganic counterions, so that micellar growth can occur at much lower surfactant and counterion concentrations.

Wormlike micelles display rich rheological behavior, often at low total surfactant concentrations (∼10^{-3} mol/L).[15−17] The entangled micellar solutions are similar to polymeric solutions, and their behavior can be best described by "living polymer" models.[18,19] However, the equilibrium and dynamics of these microstructures are determined by a delicate balance of intermolecular forces that can be easily disrupted. External changes such as temperature, dilution, variation of salt concentration, or the addition of oils or polymers can lead to the disruption of the wormlike microstructure.[19,20]

Polymerization is one route to stabilize surfactant self-assembled microstructures. Vesicles,[21] spherical micelles,[22−26] lamellae,[27] and hexagonal arrays of cylinders[28] have been polymerized, but reports of polymerizing wormlike micelles are rare.[29−31] Kline et al. reported the polymerization of rodlike micelles from cetyltrimethylammonium 4-vinylbenzoate (CTVB).[29,31] The counterions in these micelles contain a polymerizable vinyl group that binds to the hydrophilic ammonium headgroups of the wormlike micelles. Upon polymerization, the shell of linked counterions retains the cross-sectional structure of the micelles, although there is a reduction in the overall length of the polymerized micelles, possibly due to confinement of the polymerized counterions to the micellar surface.

Becerra et al.[30] reported an alternate approach to templating wormlike micelles by polymerizing styrene solubilized inside the core of micelles of the cationic surfactant cetyltrimethylammonium tosylate. This approach does not stabilize the wormlike micelle microstructure. Instead, the polymer product partially adopts the morphology of the micelle core, and the result is a mixture of empty micelles and rigid solid rods, whose length depends on the styrene-to-surfactant molar ratio.

In this paper, the structural fixation of stable wormlike micelles formed in mixtures of a polymerizable surfactant with an oppositely charged hydrotropic salt is investigated. Solutions of spheroidal micelles were prepared from the cationic surfactant, methacryloyloxyundecyltrimethylammonium bromide (MUTB), whose polymerizable methacrylate group is located in the hydrophobic tail. Micellar growth was induced by added sodium tosylate (TSNa), and the resulting wormlike micelles were then polymerized to fix their microstructure. The initial wormlike micelles and the polymerized micelles were characterized using quasi-elastic and static light scattering (QLS and SLS, respectively), NMR, small-angle neutron scattering (SANS), and cryogenic transmission electron microscopy (cryo-TEM). The wormlike micelles can be successfully polymerized to yield single-phase stable solutions of polymerized micelles whose structure and properties are insensitive to dilution. The cross-sectional radius of the wormlike assemblies (∼2 nm) does not change upon polymerization, but their length increases considerably.

Materials and Methods

Materials. Methacryloyl chloride was distilled under reduced pressure and stored at 4 °C. 11-Bromoundecanol, trimethylamine (anhydrous), sodium tosylate, anhydrous tetrahydrofuran (THF), and ethyl ether were purchased from

[†] University of Science and Technology of China.
[‡] University of Delaware.
[§] Technion−Israel Institute of Technology.
* To whom correspondence should be addressed: e-mail kaler@che.udel.edu; Tel (302) 831-3553; Fax (302) 831-6751.

10.1021/ma047646m CCC: $30.25
Published on Web 02/26/2005

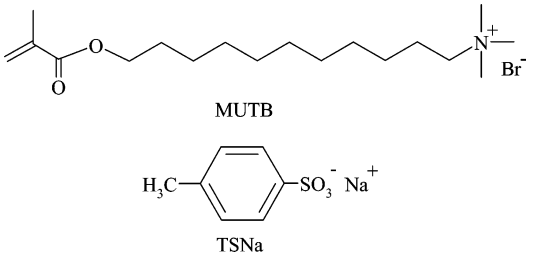

Figure 1. Chemical structures of the cationic surfactant methacryloyloxyundecyltrimethylammonium bromide (MUTB) and the hydrotropic salt sodium tosylate (TSNa).

Aldrich. The initiator 2,2′-azobis(2-methylpropionamide) dihydrochloride (V50, Wako Pure Chemical Industries, Ltd.) was recrystallized from methanol.

Preparation of MUTB. The synthesis of MUTB has been reported elsewhere.[32] Briefly, 11-bromoundecanol (20 g, 0.08 mol) and 320 mL of anhydrous THF were mixed in a flask at 0 °C under N_2, followed by the addition of 10.8 mL (0.11 mol) of methacryloyl chloride. The reaction system was bubbled with N_2 at room temperature for 2 h and left under stirring overnight. The unreacted methacryloyl chloride and solvent were removed under reduced pressure. The yellowish residue was dissolved in ethyl ether and washed with saturated sodium hydrogen carbonate solution until the aqueous layer was basic. After evaporation of the ether, a viscous yellowish liquid of 11-bromoundecyl methacrylate was obtained with a yield of 91%. MUTB with a yield of 75% was obtained by reacting 11-bromoundecyl methacrylate with trimethylamine gas in diethyl ether at 0 °C, following the procedure described by Michas et al.[33] The chemical structures of the synthesized MUTB and of TSNa are shown in Figure 1. Their structures and purity were verified by ^{1}H NMR. The spectra of these species are discussed below.

Polymerization of Wormlike Micelles. Samples for polymerization were prepared with water or D_2O and depleted of oxygen by bubbling with nitrogen for about 30 min. After dissolution at room temperature of the desired MUTB and TSNa amounts, the solution mixtures were heated to 60 °C. The water-soluble initiator V50, predissolved in degassed water or D_2O, was injected (the molar ratio of MUTB to V50 was fixed at 100), and the polymerization was carried out at 60 °C for 2 h.

QLS and SLS. QLS and SLS measurements were made using a Brookhaven BI-200SM goniometer and a BI9000AT digital correlator. Samples at 25 °C were irradiated with 488 nm light produced from a Lexel 2 W argon ion laser. QLS measurements were made at five different angles ranging from 50° to 130°. The intensity correlation data were analyzed by the method of cumulants to provide the average decay rate, $\langle\Gamma\rangle = q^2 D_a$, where D_a is the apparent diffusivity coefficient, and the normalized variance, $\nu = [\langle\Gamma^2\rangle - \langle\Gamma\rangle^2)/\langle\Gamma\rangle^2]$, which is a measure of the width of the distribution of the decay rates.[34] Here, q is the magnitude of the scattering vector given by $q = (4\pi n/\lambda)\sin(\theta/2)$, n being the refractive index of the solvent, λ the wavelength of light, and θ the scattering angle. Stock solutions of each pure surfactant were filtered through 0.22 μm Millipore Acrodisc-12 filters prior to preparing samples.

In SLS, the angular dependence of the excess absolute time-averaged scattered light intensity, known as the Rayleigh ratio $R_{vv}(q)$, of a series of diluted polymerized micellar solutions (concentrations ranging from 5.3×10^{-5} to 4.5×10^{-4} g/mL) led to the apparent weight-average molar mass $(M_w)_{app}$ and the root-mean-square z-average radius of gyration $\langle R_g^2\rangle_z^{1/2}$ (written as $\langle R_g\rangle$). The dn/dc value (0.17 mL/g) of the polymerized micelles was measured at 25 °C using an interferometric refractometer ($\lambda = 488$ nm) for a range of concentrations.

SANS. SANS measurements were made at the National Institute of Standards and Technology (NIST) in Gaithersburg, MD. An average neutron wavelength of 6 Å with a spread of 11% was used. Samples were held at 25 °C in quartz "banjo" cells with 2 mm path lengths. Three sample-to-detector distances were used to give a range in scattering vector of 0.004−0.5 Å^{-1}. The data were corrected for detector efficiency, background, and empty cell scattering and placed on an absolute scale using NIST procedures. For data analysis, the ideal model scattering curves were smeared to take into account the instrument resolution.[35] The quality of the fit is assessed from the reduced χ^2 error values between model and data.

SANS Modeling. The approximate cross-sectional radius (r_{cs}) of the micelles was obtained by analyzing the scattering data at q values beyond any interaction peaks in the scattering plots using the Guinier approximation for the form factor[36]

$$qI(q) \sim \exp(-q^2 R_{g,cs}^2/2) \tag{1}$$

where $R_{g,cs}$ is the cross-sectional radius of gyration of the cylindrical micelles and is related to the micellar cross-sectional radius by

$$r_{cs} = \sqrt{2} R_{g,cs} \tag{2}$$

More accurately, models of rigid or semiflexible cylinders were used to fit the neutron scattering spectra measured for both the original and polymerized wormlike micelles. For monodisperse rigid circular cylinders and in the absence of intermicellar interactions, the scattered intensity as a function of the scattering vector is given by[37]

$$I(q) = \frac{d\Sigma}{d\Omega}(q) = N(\rho_{cyl} - \rho_{solv})^2(\pi r_{c,s}^2 L)^2 \times \int_0^{\pi/2}\left[2\frac{\sin\left(q\frac{L}{2}\cos\alpha\right)}{q\frac{L}{2}\cos\alpha}\frac{J_1(qr_{c,s}\sin\alpha)}{qr_{c,s}\sin\alpha}\right]^2 \sin\alpha\, d\alpha \tag{3}$$

Here, $J_1(x)$ is the first-order Bessel function, α is the angle between the cylinder axis and the scattering vector q, ρ_{cyl} and ρ_{solv} are the scattering length densities of the micelle and the solvent, respectively, N is the number density of micelles, r_{cs} is the cross-sectional radius, and L is the length of the micelles. The semiflexible model used Pedersen and Schurtenberger's calculation[38] of the form factor for a wormlike chain with excluded-volume interactions. This model allows the estimation of r_{cs} as well as the contour length (L_c) and the persistence length (l_p) of the micelles, which are an indication of micellar flexibility. All other intermicellar interactions were neglected.

For both models, r_{cs} was initially set to the value calculated from the Guinier plot in order to find the adjustable parameters of L or L_c and l_p. Later, r_{cs} was also varied until a minimum for the value of χ^2 for the model fit to each SANS spectrum was found. The scattering length density (SLD) for each component was calculated by summing the scattering amplitudes of each group or atom in the molecule and dividing the total by the sum of the respective volumes. For MUTB and TSNa, the calculated SLD are 2.1×10^{-7} and 1.6×10^{-6} Å^{-2}, respectively. The scattering length density of D_2O is 6.3×10^{-6} Å^{-2}.

^{1}H NMR. ^{1}H NMR measurements were performed at 25 °C on a Bruker AC250 NMR spectrometer (resonance frequency of 250 MHz for ^{1}H).

Cryo-TEM. Prior to specimen preparation, the micellar solutions were equilibrated at 25 °C in the controlled environment vitrification system (CEVS)[39] for 20 min. Vitrified specimens were prepared on either a Quantifoil 3.5R bare grid or a 400 mesh copper grid coated with a perforated Formvar film (Ted Pella). Briefly, a small drop (~5 μL) was applied to the grid and blotted with a filter paper to form a thin liquid film of solution. The blotted sample was immediately plunged into liquid ethane at its freezing point (−196 °C) and stored under liquid nitrogen. The vitrified specimens were examined in a Philips CM120 transmission electron microscope, operated at 120 kV, using an Oxford 3500 cryo-holder maintained at below −178 °C. Images were recorded digitally on a Gatan 791 MultiScan cooled charge-coupled device (CCD) camera with

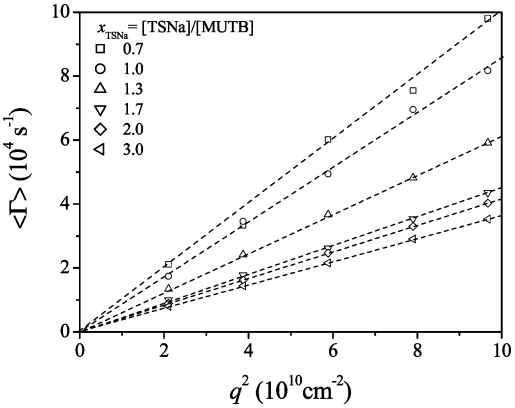

Figure 2. Average decay rates of the intensity correlation function as a function of q^2 for solutions at 50 mM MUTB and different molar ratio of TSNa, x_{TSNa}. The slopes of the lines yield the apparent diffusivity coefficients, D_a.

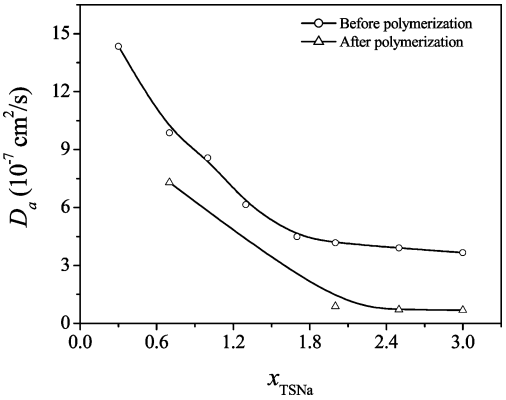

Figure 3. Apparent diffusion coefficient, D_a, before and after polymerization for solutions at 50 mM MUTB as a function of the molar ratio of TSNa, x_{TSNa}.

the Digital Micrograph software package, at low dose conditions to minimize electron beam radiation damage. Brightness and contrast enhancement were done using the Adobe Photoshop 7.0 ME package.

Results and Discussion

Formation of Wormlike Micelles and Micellar Growth. MUTB surfactant in water has a critical micelle concentration of 15 mM at 25 °C.[32] Homogeneous solutions are obtained when MUTB (≤80 mM) is mixed with TSNa up to molar ratios x_{TSNa} = [TSNa]/[MUTB] of 3.0. The counterion binding between tosylate and MUTB headgroups is not as strong as the interactions between *p*-toluidine hydrochloride (PTHC) and sodium dodecyl sulfate (SDS).[40] Upon addition of PTHC to SDS, a 1:1 complex forms in the mixed solution, and there is a region of precipitate at [PTHC]/[SDS] molar ratios > 1.0. When TSNa is added to MUTB solutions, a slightly bluish tinge appears at $x_{TSNa} \geq 1.5$, indicating an apparent micellar growth (a transition from spherical to wormlike micelles). At $x_{TSNa} = 2.0$, the critical aggregation concentration (cac) drops to 2.0 mM MUTB, as measured by surface tension. This reduction in cac is a well-known effect of adding a hydrotropic counterion salt to a surfactant solution.[41]

QLS. The elongation of the micelles upon addition of TSNa to 50 mM MUTB solutions was characterized by QLS. For all compositions, the average decay rate $\langle\Gamma\rangle$ varies linearly with q^2 (Figure 2), and the curves pass the origin. This indicates that the apparent diffusivity of the micelles, D_a, depends mostly on their translational motion, which holds true for scattering vector values $qL < 3$. Only at larger qL values is the rotational motion of the rods expected to increasingly contribute to the apparent diffusivity. Therefore, with $q = 3.1 \times 10^5$ cm^{-1} (the largest scattering vector considered), $qL < 3$ implies that the micelles should be smaller than about 100 nm. The slope of the lines in Figure 2 yields D_a, and D_a decreases with increasing x_{TSNa} (open circles, Figure 3). For a dilute suspension of rigid rods, this reduction in D_a implies an elongation of the rods.[42] Likewise, for hydrotrope−surfactant mixtures, a reduction in D_a can be interpreted as a transition from spherical to wormlike micelles of increasing length,[40] albeit the microstructure of the aggregates needs to be corroborated using complementing techniques as shown in the next sections.

To determine the length of the micelles, D_a was corrected for hydrodynamic and thermodynamic contributions. D_a can be related to the infinite dilution diffusion coefficient D_0 by

$$D_a = D_0[1 + k_D(c - \text{cac})] \tag{4}$$

where k_D is the diffusion "virial" coefficient and c is the surfactant concentration. D_0 is related to the length of the rod and its axial ratio $p = L/d$ via

$$D_0 = \frac{k_B T}{3\pi\eta L}(\ln p + \zeta) \tag{5}$$

where k_B is the Boltzmann constant, T is the absolute temperature, and η is the solvent viscosity. ζ is a function of the axial ratio p and was estimated using the Tirado et al.[43] expression of the shape factor, which is valid for axial ratios in the range of 2−30. Likewise, k_D can be expressed as[44]

$$k_D = 2MB_2 - k_f - \bar{v} \tag{6}$$

where M is the micelle molecular weight, B_2 is the osmotic second virial coefficient, which accounts for excluded-volume interactions, k_f is the hydrodynamic virial coefficient, which accounts for friction due to direct physical hindrance and/or hydrodynamic interactions, and $\bar{v}$ is the specific volume of the micelles. This analysis neglects any micelle flexibility, which is a valid assumption here since the micelles are only a few times longer than their persistence length (see SANS results below).

The above expressions are solved iteratively for L assuming that the cross-sectional radius of the micelles is preserved. The micellar core radius was set at 2.05 nm, which is approximately the length of the hydrocarbon chain of MUTB.[45] Addition of TSNa clearly causes micellar growth up to $L \sim 40$ nm at $x_{TSNa} = 3.0$ (Figure 4). For comparison, the equivalent sphere hydrodynamic diameter at each molar ratio is also shown.

NMR Studies: Counterion Adsorption. NMR is a powerful technique for investigating how the hydrotrope is associated with the micelle. The electrostatic and hydrophobic interactions between the hydrotrope counterions and the surfactant forming the micelles influence the orientation of the hydrotrope within the micelle interface. NMR measurements have shown that salicylate ions are strongly adsorbed to cetyltrimethylammonium bromide (CTAB) micelles in a configuration that allows the carboxylic and hydroxyl groups to protrude from the micelles.[15] Insertion of the hydrotrope is reflected by an upfield shift of the hydrotrope aro-

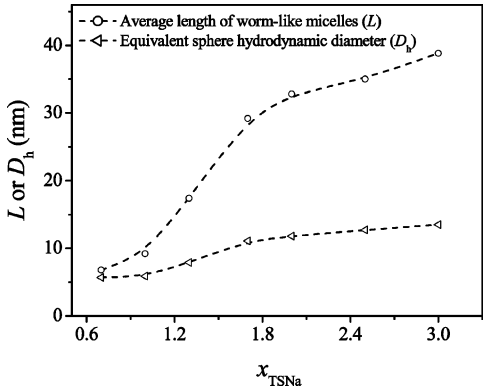

Figure 4. Average length of the unpolymerized wormlike micelles (L) and the average equivalent sphere hydrodynamic diameter (D_h) as a function of the molar ratio of TSNa, x_{TSNa}; [MUTB] = 50 mM.

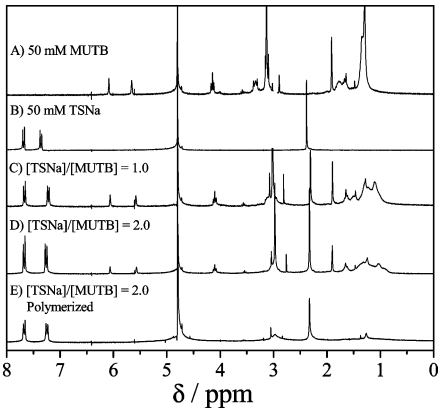

Figure 5. ^{1}H NMR spectra of (A) spherical MUTB micelles, (B) TSNa salt, (C, D) MUTB/TSNa mixtures of wormlike micelles, and (E) polymerized wormlike micelles. The MUTB concentration in the mixtures is 50 mM.

matic proton lines as well as an upfield shift of the surfactant headgroup proton resonances. A similar trend is observed in mixtures of other hydrotropes with surfactants.[40,41]

^{1}H NMR spectra of TSNa, MUTB, and their mixtures are shown in Figure 5A−D. The peak assignments of the MUTB main lines (Figure 5A) were made by comparison to spectra of cetyltrimethylammonium tosylate and similar quaternary ammonium amphiphilic methacrylates.[46,47] Within the surfactant tail, the vinyl and methacryl methyl group lines appear at δ = 5.6−6.0 and 1.9 ppm, respectively, and are important for monitoring the completion of the polymerization reaction. On the other hand, the trimethylammonium headgroup displays a large peak at 3.1 ppm due to the protons of the three methyl groups attached to the nitrogen atom. The TSNa spectrum (Figure 5B) shows the two *ortho* protons as a downfield doublet at δ = 7.7 ppm because of coupling with the *meta* protons. Likewise, the two *m*-protons appear as a doublet at δ = 7.3 ppm, while the signal for the three methyl protons at the *p*-position shows further upfield at δ = 2.4 ppm.

Upon mixing 50 mM TSNa with 50 mM MUTB (Figure 5C), the *m*-protons as well as the *p*-CH_3 resonances shift upfield from their original positions, while the positions of the *o*-proton resonances remain essentially unchanged. This indicates that the tosylate ion strongly binds to the micelles, with its *m*- and *p*-positions inserted into the micellar interior and the *o*-protons and the sulfonate atoms protruding from the micellar surface. The trimethylammonium signal also shifts upfield, further confirming that the hydrophobic portion of the tosylate intercalates between the surfactant headgroups. When the concentration of TSNa is doubled (Figure 5D), the extent of the shift for the *m*- and *p*-proton resonances is smaller compared to the extent of the shift seen for the 50 mM TSNa case. The less prominent upfield shift is probably due to the contribution of free (unbound) tosylate ions to the total signal.

Shikata et al.[48] observed a similar trend for solutions of CTAB with sodium salicylate (SS) hydrotrope. They found that when the SS concentration is low relative to the CTAB concentration, the aromatic salicylate signals move upfield relative to the position of the lines in a pure SS solution. However, these lines move back toward a lower magnetic field when the SS concentration is larger than the CTAB concentration and eventually approach the position of the lines in a SS solution. The measurements indicate the formation of a 1:1 complex of hydrotrope counterion and surfactant, for molar ratios of SS to CTAB greater than 1. Comparison of the ^{1}H NMR spectrum of MUTB and the mixtures shows that addition of TSNa to MUTB solutions broadens the resonance lines associated with hydrogen atoms in the surfactant tail below 2 ppm (Figure 5C,D). This indicates that the oil core of the wormlike micelles is less fluid (more closely packed) than that of the spherical micelles.

Cryo-TEM. Typical cryo-TEM images of the assemblies existing in solution before polymerization at 50 mM MUTB and x_{TSNA} = 2 are presented in Figure 6. In thick regions (as in Figure 6A) the structures overlap, and it is difficult to identify individual micelles and determine their shape and length. However, in thin vitrified regions (∼100 nm in thickness, Figure 6B), coexistence of small globular micelles of about 5 nm in diameter (black arrows), short and flexible wormlike micelles (black arrowheads), and a few closed micellar loops of several nanometers in diameter (white arrows) are clearly seen, indicating that before polymerization small globular micellar assemblies and wormlike micelles, smaller than 50 nm in length, are the dominant structures in solution.

Characterization of the Polymerized Wormlike Micelles. Polymerization of the wormlike micelles at different [TSNa]/[MUTB] ratios (0.7, 2.0, 2.5, and 3.0) was carried out for 2 h, at which time ^{1}H NMR showed that the reaction was complete. During polymerization, the solution mixture remained as one phase. A deepening of the bluish tinge and increasing viscosity were observed, both of which indicate qualitatively apparent micellar growth. The polymerized wormlike micellar solutions were stable for more than 7 months.

1. ^{1}H NMR Results. In the ^{1}H NMR spectrum of wormlike micelles before polymerization (Figure 5C,D), the signals at δ = 1.9 ppm (−CH_3 on the methacrylate group of MUTB surfactant) and δ = 5.6−6.0 ppm (−CH_2 on the double bond) can be clearly observed. After polymerization for 2 h, all the signals characteristic of the unsaturated double bonds have disappeared (Figure 5E), indicating complete polymerization of the double bonds of the surfactant monomers. Another interesting feature of the polymerized wormlike micelles is that the signals due to the surfactant tail at <2 ppm, and the signal of the −CH_2 protons next to the ester group (4.1 ppm), are barely noticeable, which suggests the core is

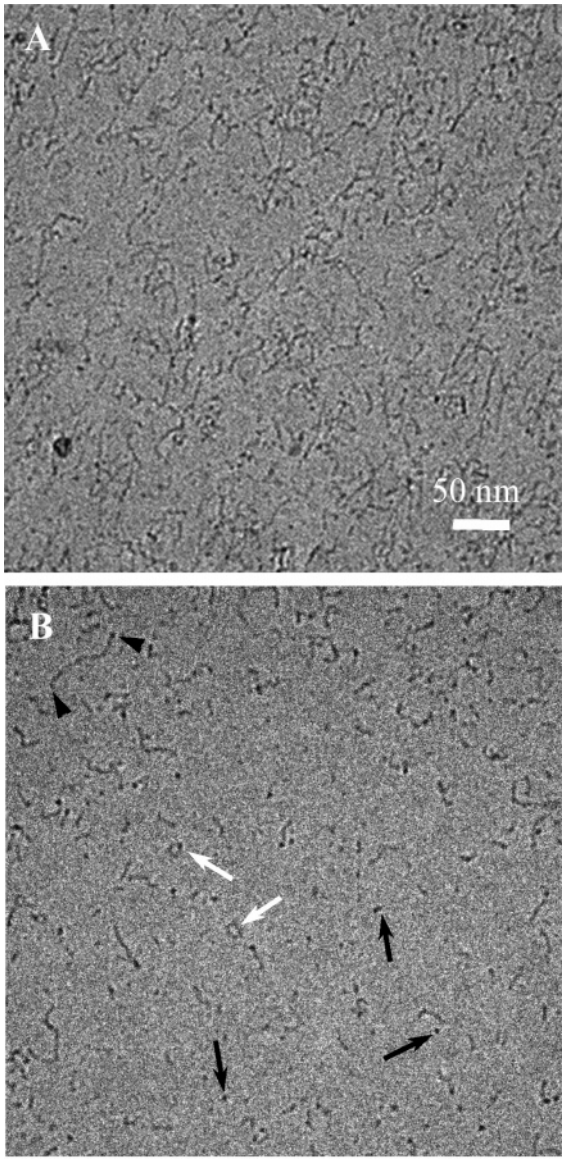

Figure 6. Cryo-TEM micrographs of the unpolymerized samples at $x_{TSNa} = 2.0$ and [MUTB] = 50 mM. The observed microstructures depend on the region of the vitrified film that is imaged. (A) Thick regions: wormlike micelles of different lengths. (B) Thin regions: small globular micelles (black arrows), flexible wormlike micelles (black arrowheads), and a few closed micellar loops of several nanometers in diameter (white arrows).

"locked" so that the mobility of the surfactant tail is greatly restricted after polymerization. This is expected given that polymerization has covalently linked the hydrophobic tails, and such line broadening is characteristic of polymerized surfactant monomers containing a reactive group on the tail.[49] The fluidity of the hydrophobic tail enclosed in the core decreases as the micelles evolve from spheres, to wormlike structures, to polymerized wormlike micelles.

2. Cryo-TEM Results. Samples at 25 °C from the viscous polymer solution containing 50 mM MUTB and $x_{TSNa} = 2.0$, and from the same sample diluted three times, that is, therefore, of much lower viscosity, were examined by cryo-TEM. In Figure 7A, the micelles appear to be cylindrical in shape and longer than those found before polymerization. However, because of the high concentration, the structures overlap. To see the individual assemblies, the sample was diluted by 3. Images of the diluted sample show several regions of mostly entangled, flexible, and probably branched micelles, coexisting with several stretched, micrometer-long cylindrical structures (black arrows, Figure 7B). These micron scale structures were not imaged in the unpolymerized samples, and they are clearly polymerized micelles. Closed rings (white arrows), several tens of nanometers in diameter, are also often seen. The smaller rings are similar to those found before polymerization, but the larger rings were not detected before, and they most likely formed upon polymerization. From these micrographs it is evident that the polymerized micelles have the same diameter as the unpolymerized micelles. Also, in Figure 7B−E the vitrified areas between the wormlike micelles are devoid of small structures. The absence of globular and short micelles, which existed before polymerization, strongly suggests that all the small assemblies were polymerized or linked to large wormlike micelles. Finally, the folded micelles seen particularly in Figure 7B,E indicate that branched micelles can also form upon polymerization.

3. QLS and SLS Results. QLS and SLS were also used to characterize the polymerized wormlike micelles. Figure 3 compares the diffusivity coefficients of wormlike micelles before and after polymerization at different x_{TSNa}. The diffusivities of the polymerized micelles were calculated following the approach discussed earlier, namely from the slope of $\langle\Gamma\rangle$ as a function of q^2. D_a decreased dramatically after polymerization, especially at higher x_{TSNa} ratios, indicating an increase in micellar length. The estimated lengths of polymerized micelles at different x_{TSNa} ratios are shown in Figure 8. The average length of the wormlike micelles polymerized at $x_{TSNa} = 2.0$ is 246 nm. Comparison with the calculated length of 34 nm for the micelles before polymerization (at $x_{TSNa} = 2.0$) indicates there is a 7-fold increase in the micellar length. Such long micelles after polymerization are not expected to be entirely rigid rods as corroborated by SANS results below. Thus, the calculated length of the polymerized micelles underestimates the true length of the micelles. During polymerization, surfactant monomers can add continuously to the propagating radical located in the core of the wormlike micelles to form much longer wormlike micelles with fixed structures.

The polymerized structures are insensitive to dilution, and D_a remains almost constant upon dilution from 50 mM MUTB to 0.5 mM MUTB (Figure 9), indicating successful "locking-in" of the wormlike micellar structure. The structure of unpolymerized wormlike assemblies typically changes with dilution, and mixed micelles disassociate into unimers at concentrations below the critical aggregation concentration (2.0 mM, at $x_{TSNa} = 2.0$). The successful capture of a stable wormlike micellar structure was also confirmed by the similar D_a value measured after dialysis of the polymerized wormlike micelle solutions against deionized water.

Since the structure of the wormlike micelle does not change with dilution, SLS can be used to measure the molar mass and the radius of gyration of the polymerized wormlike micelles. A Zimm plot analysis (Figure 10) yields a weight-average micelle molar mass of about 5.0×10^6 g mol^{-1}. This value corresponds to approximately 11 000 MUTB surfactant molecules in each polymerized micelle, assuming that all the surfactant molecules have participated in the formation of the

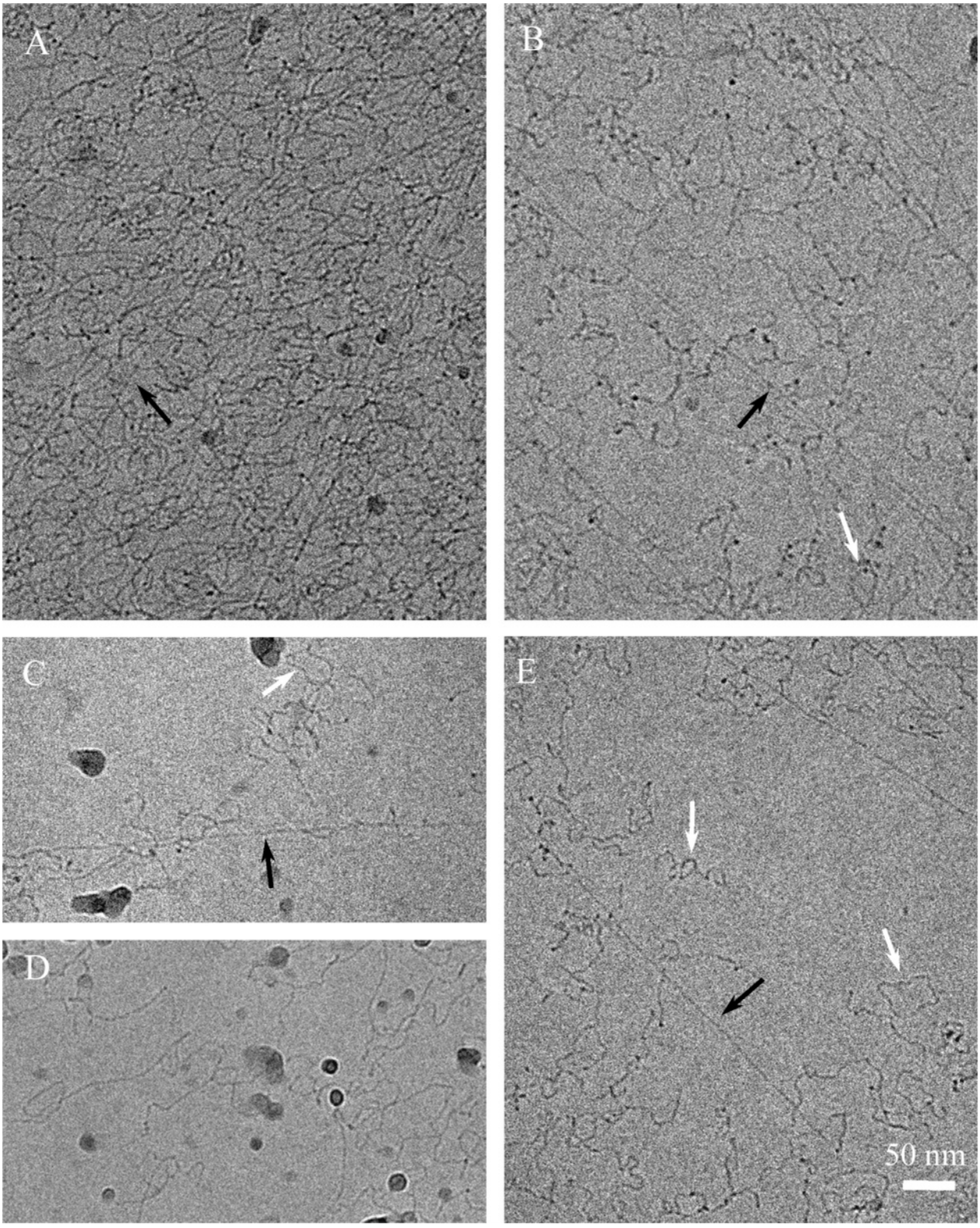

Figure 7. Micrographs of the polymerized micelles ($x_{TSNa} = 2.0$ and [MUTB] = 50 mM). (A) Under no dilution, long overlapping structures are observed. (B−E) After three times dilution, individual assemblies are evident such as numerous flexible micelles, some stretched, micrometer-long cylindrical micelles (black arrows), and large closed loops (white arrows).

polymerized wormlike micelles and assuming the formation of a 1:1 complex between MUTB surfactant headgroups and the tosylate counterions. The *z*-average hydrodynamic radius of gyration ($\langle R_g \rangle$) of the polymerized wormlike micelles is 108 nm, and the equivalent sphere hydrodynamic radius ($\langle R_h \rangle$) for the same sample is 29 nm; thus, $\langle R_g \rangle / \langle R_h \rangle = 3.7$. This ratio, which depends on the particle shape and density profile of the scattering objects, is about 1.5 for monodisperse random coils,[50] while for elongated micelles it varies in the range of 1.3−4.0.[51] Here, the high value of $\langle R_g \rangle / \langle R_h \rangle$ is consistent with an extended wormlike microstructure.

4. SANS Results. SANS was used to characterize the unpolymerized (open squares) and polymerized (open triangles) wormlike micelles in D_2O at 50 mM MUTB and $x_{TSNa} = 2.0$ (Figure 11). The spectra for the

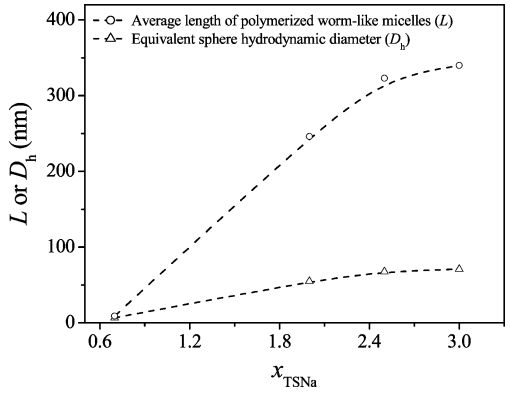

Figure 8. Average length of the polymerized wormlike micelles (L) and the average equivalent sphere hydrodynamic diameter (D_h) as a function of the molar ratio of TSNa, x_{TSNa}; [MUTB] = 50 mM.

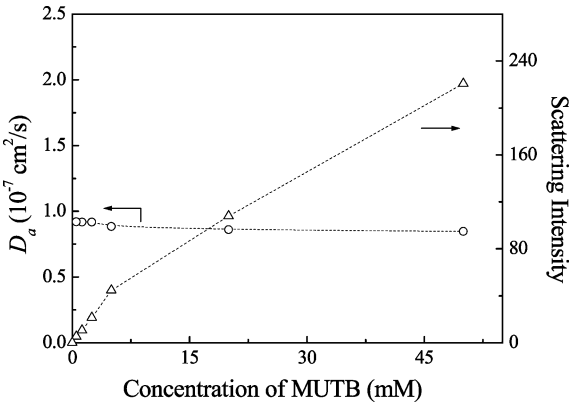

Figure 9. Apparent diffusion coefficient, D_a, and scattering intensity upon dilution for wormlike micelles polymerized at 50 mM MUTB and $x_{TSNa} = 2.0$.

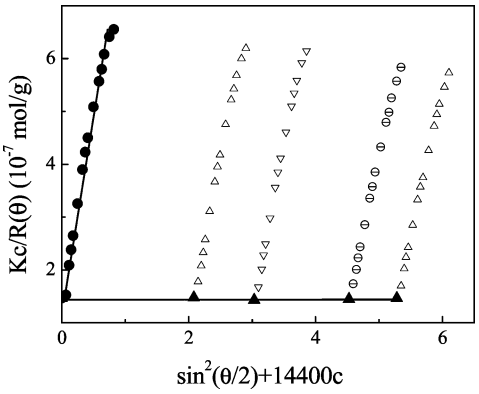

Figure 10. Zimm plot of polymerized micelles (polymerized at 50 mM MUTB and a molar ratio, $x_{TSNa} = 2.0$). A series of dilute polymerized solutions (concentrations ranging from 5.3 $\times$ 10^{-5} to 4.5 $\times$ 10^{-4} g/mL) were used for the static light scattering measurements.

unpolymerized and polymerized micelles display a q^{-1} dependence at intermediate q values, which is a signature of scattering from cylindrical objects. The spectra are thus qualitatively consistent with the presence of wormlike micelles in solution before and after polymerization. Because of the screening effect of TSNa salt, the neutron scattering profiles do not show an interaction peak at lower q values such as often arises in spectra from micellar solutions of alkyltrimethylammonium surfactants.

The spectrum of the polymerized micelles overlaps at intermediate and high q values with that of the micelles

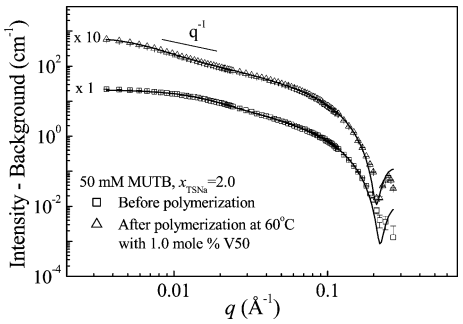

Figure 11. SANS spectra for the (□) unpolymerized and (△) polymerized wormlike micelles in D_2O. A semiflexible cylinder model with three adjustable parameters is used to fit both spectra (solid lines; Table 1). The spectrum of the polymerized wormlike micelles is shifted upward by a factor of 10 for clarity.

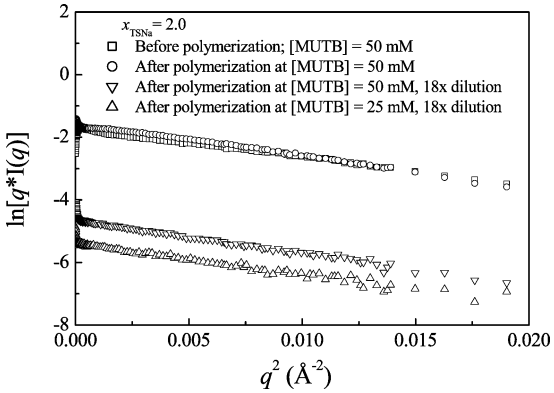

Figure 12. Cross-sectional Guinier plots for unpolymerized micelles, polymerized wormlike micelles, and polymerized wormlike micelles after 18 times dilution.

before polymerization, suggesting that the cross-sectional radius of the micelles is preserved during polymerization. After polymerization, an increase of the scattering in the low-q region is observed, which indicates an increase in length of the wormlike micelles. These results qualitatively confirm that the cross-sectional structure of the wormlike micelles has been preserved during polymerization and that the length of the micelles increases.

The cross-sectional radius of the micelles is first obtained by analyzing the intermediate-q portions of the scattering curves using the Guinier approximation for the form factor. Guinier plots are shown in Figure 12 for the original (open squares) and polymerized micelles (open circles). From the fitted linear portions of the curves, the unpolymerized and polymerized micelles have a micellar radius of 1.9 and 2.0 nm, respectively. These are in good agreement with the calculated length of a fully extended MUTB molecule of 2.05 nm (which was used in the light scattering calculations above).

The scattering data before polymerization can be best fit using a semiflexible cylinder model, giving a cross-sectional radius r_{cs} of 1.7 nm, a contour length L_c of 41.3 $\pm$ 0.9 nm, and a persistence length l_p of 12.2 $\pm$ 0.7 nm. The results are summarized in Table 1. Note that the length of the wormlike micelles obtained from QLS (34 nm, Figure 4) is in agreement with the contour length from SANS fitting. Fitting the scattering data of the polymerized micelles to a semiflexible cylinder model yields $r_{cs} = 1.8$ nm, $L_c = 127 \pm 5$ nm, and $l_p = 24 \pm 1$ nm (Table 1). Thus, SANS results show that polymerization increases the length of the wormlike micelles from about 40 to 130 nm.

Table 1. Results of Fitting the Semiflexible Cylindrical Model to SANS Spectra of the Initial Wormlike Micelles, the Polymerized Wormlike Micelles, and Polymerized Micelles after Dilution[a]

sample description	r_{cs} (nm) (Guinier)	r_{cs} (nm) (fitting)	L_c (nm)	l_p (nm)
[MUTB] = 50 mM, unpolymerized	1.9	1.7	41.3 ± 0.9	12.2 ± 0.7
[MUTB] = 50 mM, polymerized	2.0	1.8	127 ± 5	24 ± 1
[MUTB] = 50 mM, polymerized and diluted 18 times	2.1	2.0	187	23
[MUTB] = 25 mM, polymerized and diluted 18 times	2.1	2.1	227	25

[a] In all entries, [TSNa]/[MUTB] = 2.0.

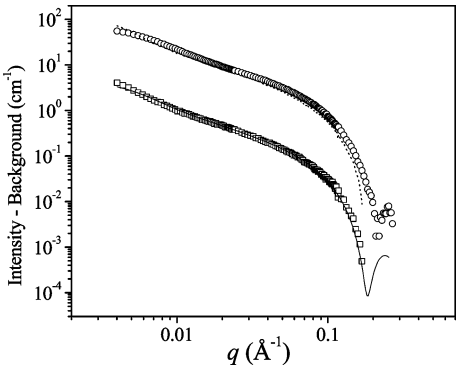

Figure 13. SANS spectra for the (○) original polymerized wormlike micelles (no dilution) and (□) the same polymerized micelles after 18 times dilution. The solid line represents the best fit to the experimental data using a semiflexible model with excluded volume interactions (Table 1). The dotted line is the scattering profile of the diluted sample times a factor of 18 and overlaps the experimental data of the undiluted micellar solution.

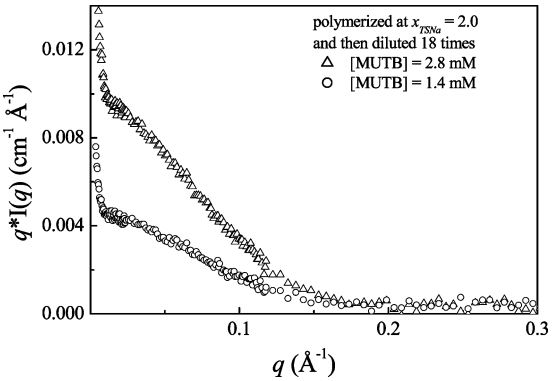

Figure 14. Holtzer plot of polymerized wormlike micelles polymerized at different MUTB concentrations and then diluted 18 times. The upturn at low q values indicates a semiflexible wormlike microstructure.

Neutron scattering measurements of this polymerized sample after 18 times dilution ([MUTB] = 2.8 mM) are displayed in Figure 13. The results from the Guinier analysis and from the best fit using the semiflexible model are summarized in Table 1. When the scattered intensity of this dilute sample is multiplied by 18, the scattering profile of the nondiluted sample is recovered (Figure 13). Since the scattered intensity of the diluted and nondiluted samples scales linearly with dilution, the structure factor of the assemblies is one. This result confirms it is appropriate to neglect intermicellar interactions other than the excluded-volume interactions, as is done in the analysis above.

Evidence of the flexibility of the micelles is obtained from a Holtzer plot (Figure 14), which is constructed to highlight the deviation of the scattering data from that of ideal, rigid cylinders. In this plot, the upturn in the low-q region indicates the micelles are best described by a semiflexible cylinder model. A similar upturn is also observed for a second sample originally polymerized at 25 mM of MUTB and $x_{TSNa} = 2.0$ and also diluted by 18 times so that [MUTB] = 1.4 mM. In this case, the best fit (Table 1) gives a radius and persistence length similar to that of the sample polymerized at [MUTB] = 50 mM. This suggests that the radius and rigidity of the polymerized micelles might not depend on the initial amount of monomer. Modeling of any of these data using the rigid cylinder model gave poor quality fits at low q values. Similarly, a model-independent analysis using the indirect Fourier transform method could not provide information on the length of the micelles because the estimated lengths are larger than π/q_{min}, which is the maximum length scale that can be probed using this approach.[52,53]

Mechanism. Several groups have observed micellar growth during polymerization of spherical micelles. Cochin et al. proposed a mechanism for micellar polymerization that completely excludes a topological polymerization of spherical micelles.[25] Their mechanism considers the dynamic nature of the micelles and the degree of reactivity of the polymerizable group, and a similar approach can account for the growth of the micelles. The interplay of the variables presented below favors micellar growth for the case of mixtures with a low cac, whose surfactants contain a polymerizable group of high reactivity such as methacrylate, located within the tail. Other scenarios require a different treatment as reviewed elsewhere.[25]

The dynamic nature of the micelle is best described in terms of the micelle lifetime and the time for the association of surfactant monomers into the micelles. During polymerization the mean lifetime of the initial micelles is given by[54]

$$t_m = N\tau_2 a\left[1 + \frac{\sigma^2}{N}a\right]^{-1} \tag{8}$$

where N is the average aggregation number of the micelles, $a = (c - \text{cac})/\text{cac}$ is a solubility term given by the concentration of surfactant (c) and the cac of the mixture, σ is the standard deviation of the aggregation number distribution, and τ_2 is the relaxation time associated with the formation−breakdown of the micelles. σ^2/N is typically close to 1[55] and far from the cac, $a \gg 1$, so that eq 8 reduces to

$$t_m = N\tau_2 \tag{9}$$

which is applicable here, since the cac = 2 mM for solutions made at $x_{TSNa} = 2.0$.

The relaxation time τ_2, as determined by various methods, can vary over a broad range (1−500 ms) depending on concentration, temperature, or surfactant chain length.[55] A good approximation for cationic surfactants with chain length between 14 and 16 carbon atoms and $T > 40$ °C is τ_2 in the range of 1−20 ms.[25] N is easily calculated from the micelle and surfactant dimensions, and for the 34 nm long unpolymerized

micelles $N \approx 1100$ (MW $\sim 5 \times 10^5$). Therefore, from eq 9, $t_m \approx 1-20$ s. This time is considerably longer than typical spherical micelle lifetimes of $10^{-2}-10^{-1}$ s.[25]

In addition, the aggregation number of the micelles fluctuates around N due to the diffusion of surfactant monomers in to and out of the micelle. This flow of surfactant is important since unreacted monomer can migrate from one micelle to another during the course of the reaction. The time scale for association of a monomer species, t_a, is given by $(k^+\text{cac})^{-1}$, where the association rate constant is $k^+ \approx 10^9$ (M s)$^{-1}$.[55] Thus, $t_a \approx 5 \times 10^{-7}$ s, so that monomers are continuously entering micelles and can potentially be incorporated into the growing chain of an initiated micelle.

Lastly, the speed at which an oligomeric chain grows mainly depends on the time it takes a monomer to add to the growing chain. This time is given by $t_p = (k_p[M])^{-1}$ where $k_p \approx 1000$ (M s)$^{-1}$ for n-alkyl methacrylates, $n > 10$, and [M] is the monomer concentration.[56] For the solutions at [MUTB] = 50 mM, $t_p = 2 \times 10^{-2}$ s at the beginning of the reaction, a value which is 2 orders of magnitude shorter than the micelle lifetime of 1−20 s but much longer than the time for the association of a surfactant monomer to a micelle.

Radicals formed by the decomposition of water-soluble initiators rapidly partition into micelles. The entry of these radicals probably follows the Maxwell−Morrison model for radical entry in emulsion polymerization.[57] In microemulsion polymerization,[58] this model has accounted well for the entry of radicals into the monomer-swollen micelles and seems applicable here, since the methacryloyl group of the polymerizable surfactant is condensed at the core of the micelles. In addition, the number of micelles far exceeds the number of radicals, and therefore the probability of more than one radical entering a micelle is negligible.

Because the time required for a propagation step is shorter than the average micelle lifetime, oligomeric radicals form during the average micelle lifetime. The length of these oligomeric radicals, given by the ratio of t_m/t_p calculated above, is 50−1100 units. These oligomers polymerized within the core of the micelles likely fix the micelle radius. As shown above, the time required for the association of a surfactant monomer to a micelle is much shorter than the time required for a monomer to incorporate to the growing radical. Thus, the uniaxial growth of these chains results from the addition of monomeric surfactant from unnucleated micelles to oligomeric micelles and proceeds until the reaction reaches nearly complete conversion. The growth of these oligomeric chains gives rise to a polymer of high molecular weight.

Conclusions

Addition of the hydrotropic salt sodium tosylate (TSNa) to solutions of a polymerizable cationic surfactant, methacryloyloxyundecyltrimethylammonium bromide (MUTB), leads to a transition from spherical to wormlike micelles. The intercalation of the hydrophobic portion of the tosylate with the surfactant headgroups drives this micellar elongation phenomenon. The wormlike micelles are then polymerized to "lock-in" the threadlike architecture, and longer wormlike micelles with the same cross-sectional radius as the unpolymerized micelles are obtained after polymerization. A mechanism that considers the dynamic nature of the micelles and the speed of the propagation step can account for the growth of the micelles.

Acknowledgment. We acknowledge the support of the National Science Foundation CTS-9814399. The National Institute of Standards and Technology, Gaithersburg, MD, provided neutron scattering facilities used in this work. P. A. Hassan, G. M. Santonicola, and S. R. Kline provided insightful comments about scattering data analysis. The cryo-TEM studies were performed at the "Cryo-TEM Hannah and George Krumholz Laboratory for Advanced Microscopy" at the Technion, part of the "Technion Project on Complex Fluids".

References and Notes

(1) Magid, L. J.; Li, Z.; Butler, P. D. *Langmuir* **2000**, *16*, 10028−10036.
(2) Magid, L. J. *J. Phys. Chem. B* **1998**, *102*, 4064−4074.
(3) Khatory, A.; Lequeux, F.; Kern, F.; Candau, S. J. *Langmuir* **1993**, *9*, 1456−1464.
(4) Aswal, V. K.; Goyal, P. S. *Phys. Rev. E* **2000**, *61*, 2947−2953.
(5) Ali, A. A.; Makhloufi, R. *Phys. Rev. E* **1997**, *56*, 4474−4478.
(6) Rehage, H.; Hoffmann, H. *J. Phys. Chem.* **1988**, *92*, 4712−4719.
(7) Soltero, J. F. A.; Puig, J. E.; Manero, O. *Langmuir* **1996**, *12*, 2654−2662.
(8) Carver, M.; Smith, T. L.; Gee, J. C.; Delichere, A.; Caponetti, E.; Magid, L. J. *Langmuir* **1996**, *12*, 691−698.
(9) Mishra, B. K.; Samant, S. D.; Pradhan, P.; Mishra, S. B.; Manohar, C. *Langmuir* **1993**, *9*, 894−898.
(10) Imae, T.; Kamiya, R.; Ikeda, S. *J. Colloid Interface Sci.* **1985**, *108*, 215−225.
(11) Yatcilla, M. T.; Herrington, K. L.; Brasher, L. L.; Kaler, E. W.; Chiruvolu, S.; Zasadzinski, J. A. *J. Phys. Chem.* **1996**, *100*, 5874−5879.
(12) Soderman, O.; Herrington, K. L.; Kaler, E. W.; Miller, D. D. *Langmuir* **1997**, *13*, 5531−5538.
(13) Hyde, A. J.; Johnstone, D. W. M. *J. Colloid Interface Sci.* **1975**, *53*, 349−357.
(14) Balasubramanian, D.; Srinivas, V.; Gaikar, V. G.; Sharma, M. M. *J. Phys. Chem.* **1989**, *93*, 3865−3870.
(15) Manohar, C.; Rao, U. R. K.; Valaulikar, B. S.; Iyer, R. M. *J. Chem. Soc., Chem. Commun.* **1986**, 379−381.
(16) Candau, S. J.; Hirsch, E.; Zana, R.; Adam, M. *J. Colloid Interface Sci.* **1988**, *122*, 430−440.
(17) Lin, Z. *Langmuir* **1996**, *12*, 1729−1737.
(18) Cates, M. E. *Macromolecules* **1987**, *20*, 2289−2296.
(19) Hoffmann, H.; Ulbricht, W. *J. Colloid Interface Sci.* **1989**, *129*, 388−405.
(20) Brackman, J. C.; Engberts, J. *J. Am. Chem. Soc.* **1990**, *112*, 872−873.
(21) Paleos, C. M. *Polymerization in Organized Media*; Gordon and Breach: Philadelphia, 1992.
(22) Larrabee, C. E.; Sprague, E. D. *J. Polym. Sci., Part C: Polym. Lett.* **1979**, *17*, 749−757.
(23) Lerebours, B.; Perly, B.; Pileni, M. P. *Chem. Phys. Lett.* **1988**, *147*, 503−508.
(24) Hamid, S.; Sherrington, D. *J. Chem. Soc., Chem. Commun.* **1986**, 936−938.
(25) Cochin, D.; Zana, R.; Candau, F. *Macromolecules* **1993**, *26*, 5765−5771.
(26) Hamid, S. M.; Sherrington, D. C. *Polymer* **1987**, *28*, 332−339.
(27) McGrath, K. M.; Drummond, C. J. *Colloid Polym. Sci.* **1996**, *274*, 316−333.
(28) Thundathil, R.; Stoffer, J. O.; Friberg, S. E. *J. Polym. Sci., Part A: Polym. Chem.* **1980**, *18*, 2629−2640.
(29) Kline, S. R. *Langmuir* **1999**, *15*, 2726−2732.
(30) Becerra, F.; Soltero, J. F. A.; Puig, J. E.; Schulz, P. C.; Esquena, J.; Solans, C. *Colloid Polym. Sci.* **2003**, *282*, 103−109.
(31) Gerber, M. J. K. S. R.; Walker, L. M. *Langmuir* **2004**, *20*, 8510−8516.
(32) Liu, S. Y.; Gonzalez, Y. I.; Kaler, E. W. *Langmuir* **2003**, *19*, 10732−10738.
(33) Michas, J.; Paleos, C. M.; Dais, P. *Liq. Cryst.* **1989**, *5*, 1737−1745.
(34) Koppel, D. E. *J. Chem. Phys.* **1972**, *57*, 4814.
(35) Barker, J. G.; Pedersen, J. S. *J. Appl. Crystallogr.* **1995**, *28*, 105−114.
(36) Koehler, R. D.; Raghavan, S. R.; Kaler, E. W. *J. Phys. Chem. B* **2000**, *104*, 11035−11044.

(37) Guinier, A.; Fournet, G. *Small-Angle Scattering of X-rays*; John Wiley and Sons: New York, 1955.
(38) Pedersen, J. S.; Schurtenberger, P. *Macromolecules* **1996**, *29*, 7602−7612.
(39) Bellare, J. R.; Davis, H. T.; Scriven, L. E.; Talmon, Y. *J. Electron Microsc. Tech.* **1988**, *10*, 87−111.
(40) Hassan, P. A.; Raghavan, S. R.; Kaler, E. W. *Langmuir* **2002**, *18*, 2543−2548.
(41) Bhat, M.; Gaikar, V. G. *Langmuir* **1999**, *15*, 4740−4751.
(42) Broersma, S. *J. Chem. Phys.* **1960**, *32*, 1626−1631.
(43) Tirado, M. M.; Martinez, C. L.; Delatorre, J. G. *J. Chem. Phys.* **1984**, *81*, 2047−2052.
(44) Russo, P. S.; Karasz, F. E.; Langley, K. H. *J. Chem. Phys.* **1984**, *80*, 5312−5325.
(45) Tanford, C. *The Hydrophobic Effect: Formation of Micelles and Biological Membranes*, 2nd ed.; John Wiley & Sons: New York, 1980.
(46) Soltero, J. F. A.; Puig, J. E.; Manero, O.; Schulz, P. C. *Langmuir* **1995**, *11*, 3337−3346.
(47) Hamid, S. M.; Sherrington, D. C. *Polymer* **1987**, *28*, 325−331.
(48) Shikata, T.; Hirata, H.; Kotaka, T. *Langmuir* **1988**, *4*, 354−359.
(49) Summers, M.; Eastoe, J.; Richardson, R. M. *Langmuir* **2003**, *19*, 6357−6362.
(50) Cohen, D. E.; Thurston, G. M.; Chamberlin, R. A.; Benedek, G. B.; Carey, M. C. *Biochemistry* **1998**, *37*, 14798−14814.
(51) Burger, C.; Hao, J.; Ying, Q. *J. Colloid Interface Sci.* **2004**, *275*, 632−641.
(52) Glatter, O. *J. Appl. Crystallogr.* **1979**, *12*, 166−175.
(53) Glatter, O. *J. Appl. Crystallogr.* **1980**, *13*, 577−584.
(54) Aniansson, G. E. A. *Prog. Colloid Polym. Sci.* **1985**, *70*, 2−5.
(55) Aniansson, E. A. G.; Wall, S. N.; Almgren, M.; Hoffmann, H.; Kielmann, I.; Ulbricht, W.; Zana, R.; Lang, J.; Tondre, C. *J. Phys. Chem.* **1976**, *80*, 905−922.
(56) Hutchinson, R. A.; Beuermann, S.; Paquet, D. A.; McMinn, J. H. *Macromolecules* **1997**, *30*, 3490−3493.
(57) Maxwell, I. A.; Morrison, B. R.; Napper, D. H.; Gilbert, R. G. *Macromolecules* **1991**, *24*, 1629−1640.
(58) Morgan, J. D.; Kaler, E. W. *Macromolecules* **1998**, *31*, 3197−3202.

MA047646M